points marked T_g^v and T_m^v, where the curve G-G′ intersects C-C′, the crystalline and liquid phases have the same molar volume or density. Beyond these points the crystal would be less dense than its liquid phase at the same temperature and for a close-packed crystal this is quite unexpected. These two points therefore represent further catastrophe points, the boundaries of regions of paradox comparable to those of Kauzmann. (There are materials for which the density of the liquid exceeds that of the crystalline solid[6], including Ga, Bi, Sb, H_2O and KI at elevated pressure, but these cases arise from the occurrence of a very open crystalline structure.)

Having identified the two isochoric catastrophe points at which crystal and liquid possess the same density and which preempt the isentropic catastrophe points, I can estimate from these entropy curves the molar volumes of the two phases as they vary with temperature. The object of this last calculation is to locate the point of rigidity instability which, according to the above ideas, occurs where the density of the superheated crystal equals that of the liquid at the freezing point. For a non-isothermal process

$$\Delta S = \alpha_v \beta_T \Delta V + \int (C_v/T)\,dT$$

$$\approx \alpha_v \beta_T \Delta V + C_v \ln(T/T_0) \qquad (3)$$

The latter approximation applies if C_v is constant, as may be assumed well above the Debye temperature. Taking T_0 as T_m, the crystalline and liquid volumes are estimated from curves G-G′ and C-C′ by subtracting $C_v \ln(T/T_m)$ and dividing by $\alpha_v \beta_T$. These are plotted as the dashed lines in Fig. 2, to which the volume scale on the right-hand side applies. The point T_m^r at which the volume of the superheated crystal equals the volume of the liquid at the freezing point is marked. This is the point at which the rigidity modulus vanishes and shear instability occurs, and this precedes both other catastrophe points T_m^v and T_m^s. I note that the calculations of Boyer[15] indicate that the occurrence of a shear instability drives a preemptive instability in the compressibility. Thus, for crystalline superheating a succession of catastrophes occur in the sequence thermodynamic (equilibrium melting), elastic compressibility, elastic rigidity, isochoric (equal volumes for crystal and liquid) and finally, entropic points. I believe that the last two catastrophes are not observable as they are preceded by the rigidity catastrophe which is the underlying cause of melting. □

Received 2 June; accepted 17 October 1989.

1. Lindemann, F. A. *Z. Phys.* **11**, 609-615 (1910).
2. Born, M. *J. Chem. Phys.* **7**, 591-601 (1939).
3. Fecht, H. J. & Johnson, W. L. *Nature* **334**, 50-51 (1988).
4. Kauzmann, W. *Chem. Rev.* **43**, 219-256 (1948).
5. Cohen, M. H. & Grest, G. S. *Phys. Rev.* B**20**, 1077-1098 (1979).
6. Ubbelohde, A. R. *The Molten State of Matter* (Wiley, Chichester, 1978).
7. Tallon, J. L., Robinson, W. H. & Smedley, S. I. *J. phys. Chem.* **82**, 1277-87 (1978).
8. Tallon, J. L., Robinson, W. H. & Smedley, S. I. *Nature* **266**, 337-338 (1977).
9. Tallon, J. L. *Phil. Mag.* A**39**, 151-161 (1979).
10. Abraham, F. F. *Phys. Rep.* **80**, 339-374 (1981).
11. Kosterlitz, J. M. & Thouless, D. J. *J. Phys.* C**5**, L124-126 (1972); C**6**, 1181-1191 (1973).
12. Tallon, J. L. & Robinson, W. H. *Phys. Lett.* A**87**, 365-368 (1982).
13. Tallon, J. L. *Phys. Rev.* B**29**, 4153-4155 (1984).
14. Madsen, J. U. & Cotterill, R. M. J. *Phys. Lett.* A**83**, 219-220 (1981).
15. Boyer, L. L. *Phase Transitions* **5**, 1-48 (1985).

ACKNOWLEDGEMENTS. I thank the New Zealand DSIR for a study award to visit Cambridge University, where this work was carried out.

Interhemispheric asymmetry in climate response to a gradual increase of atmospheric CO_2

R. J. Stouffer, S. Manabe & K. Bryan

Geophysical Fluid Dynamics Laboratory/NOAA, Princeton University, Princeton, New Jersey 08542, USA

THE transient response of a coupled ocean–atmosphere model to an increase of atmospheric carbon dioxide has been the subject of several studies[1–8]. The models used in these studies explicitly incorporate the effect of heat transport by ocean currents and are different from the model used by Hansen *et al.*[9]. Here we evaluate the climatic influence of increasing atmospheric carbon dioxide using a coupled model recently developed at the NOAA Geophysical Fluid Dynamics Laboratory. The model response exhibits a marked and unexpected interhemispheric asymmetry. In the circumpolar ocean of the Southern Hemisphere, a region of deep vertical mixing, the increase of surface air temperature is very slow. In the Northern Hemisphere of the model, the warming of surface air is faster and increases with latitude, with the exception of the northern North Atlantic, where it is relatively slow because of the weakening of the thermohaline circulation.

The model we use here consists of general circulation models (GCMs) of the atmosphere and oceans and a simple model of the continental surface that involves the budgets of heat and water. It is a global model and includes realistic geography. The atmospheric component of the model used here is very similar to the model used in ref. 10. The seasonally varying insolation at the top of the model atmosphere is taken into account in calculating the solar radiation. Whenever the relative humidity at a grid point exceeds a critical value (99%), the grid box is filled with cloud; otherwise, it is free of cloud. The atmospheric GCM uses a spectral transform method in which the horizontal distributions of predicted variables are represented by spherical harmonics (15 associated Legendre functions for each of 15 Fourier components) and grid-point values. For vertical-finite-difference calculations, nine unequally spaced levels are chosen. The ocean GCM uses a full finite-difference technique and has a regular grid system with 4.5°×3.75° (latitude×longitude) spacing and 12 vertical levels[11]. The atmospheric and oceanic components of the model interact with each other continuously through the exchange of heat, water and momentum fluxes.

Two 100-year integrations of the coupled model were performed. In the first integration the atmospheric concentration of carbon dioxide increased by the rate of 1% yr^{-1} (compounded). The CO_2 concentration remains unchanged in the second integration (the control). We have evaluated the influence of

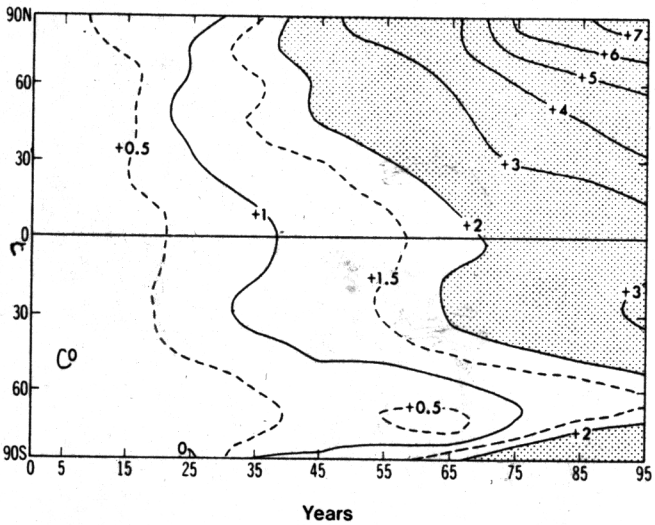

FIG. 1 Latitude–time distribution of the difference in zonally averaged, decadal-mean surface air temperature (°C) between the two integrations. Zonal-mean surface air temperature is averaged over the decades centred at the fifth, fifteenth . . ., and ninety-fifth year of the experiment.

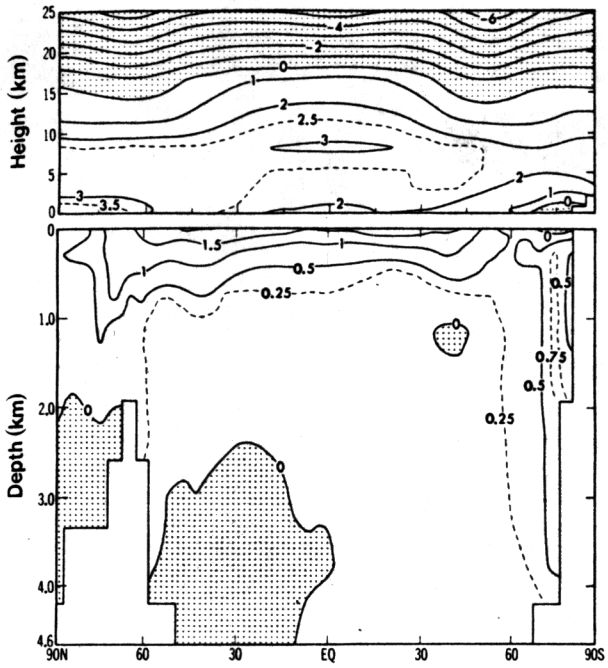

FIG. 2 Zonal-mean difference in temperature (°C) of the ocean–atmosphere model between the two integrations. The difference represents the decadal average over years 61–70. The atmospheric data have been interpolated to isobaric surfaces.

gradually increasing atmospheric carbon dioxide upon the coupled system from the difference between the first and second (control) integrations. If the CO_2 increase of 1% yr^{-1} begins in AD 1958, the doubling of CO_2 concentration would be achieved around AD 2030. Such an increase of CO_2 is larger than its projected increase but is approximately equal to the present rate of increase of the combined thermal forcing of all greenhouse gases (other than water vapour)[12].

The initial conditions for both integrations have realistic seasonal and geographical distributions of surface temperature, surface salinity and sea ice, with which both the atmospheric and oceanic components of the model are nearly in equilibrium. This quasi-equilibrium condition was obtained by separate time integrations of these two components of the model using observed surface conditions. The convergence of the oceanic component towards equilibrium was accelerated by the method described in ref. 13.

To avoid the systematic climate drift caused by the bias of the model during the two 100-year integrations, the oceanic surface fluxes of heat and water are adjusted seasonally and geographically, but not interannually, using the method described in ref. 14. Identical adjustments are applied to both the first and the second integrations defined above. By contrast to recent studies[4,8], no systematic trends are evident during the control integration, indicating that the initial condition is close to stable equilibrium and the flux adjustments are working as expected.

Figure 1 shows the latitude–time distribution of the CO_2-induced change of zonally averaged, decadal-mean surface air temperature during the 100-year experiment. In the Northern Hemisphere the warming of surface air increases with latitude, partly because of the poleward retreat of both snow cover and sea ice which have high surface albedo. The relatively large warming in high northern latitudes is essentially confined to the lower troposphere because of the stable stratification. This is indicated in Fig. 2 which shows the difference in zonal-mean temperature between the two integrations for the seventh decade of the experiment. The ocean warming is essentially confined to the upper layer, except near Antarctica. It also increases with latitude in the Northern Hemisphere, but becomes small near the North Pole which is covered by sea ice.

The meridional profile of the near-surface warming in the Northern Hemisphere is qualitatively similar to the difference between two equilibrium climates of a model with the normal and the above-normal concentrations of atmospheric CO_2. (See, for example, refs 15, 16, studies that were conducted using an atmosphere/mixed-layer-ocean model and atmosphere–ocean GCM, respectively.)

Over the northern North Atlantic, the increase of surface air temperature is significantly smaller than the zonal average. This is evident in Fig. 3 which shows the geographical distribution of the difference in decadal-mean surface air temperature between the two integrations for the seventh decade of the experiment. Because of the increase in runoff and precipitation over evaporation, surface salinity decreases and the stability of upper ocean layer increases in the northern North Atlantic. Thus, the thermohaline circulation of the North Atlantic is weakened by ~25% by the seventh decade of the experiment. The weakening is shown in Fig. 4 which illustrates the meridional circulation zonally averaged over the entire oceanic segment of a latitude circle. (Note the reduction from 16 to 12 Sv in the Northern Hemisphere.) Because of the weakening of the thermohaline circulation, the northward advection of warm and saline subtropical surface water is reduced, thereby reducing surface salinity further and making the increase of sea surface temperature relatively small over the northern North Atlantic Ocean as indicated in Fig. 3. The reduction of surface salinity stabilizes the near-surface layer and provides a feedback that further weakens the thermohaline circulation in the northern North Atlantic.

In an earlier study, Bryan and Spelman[3] investigated the

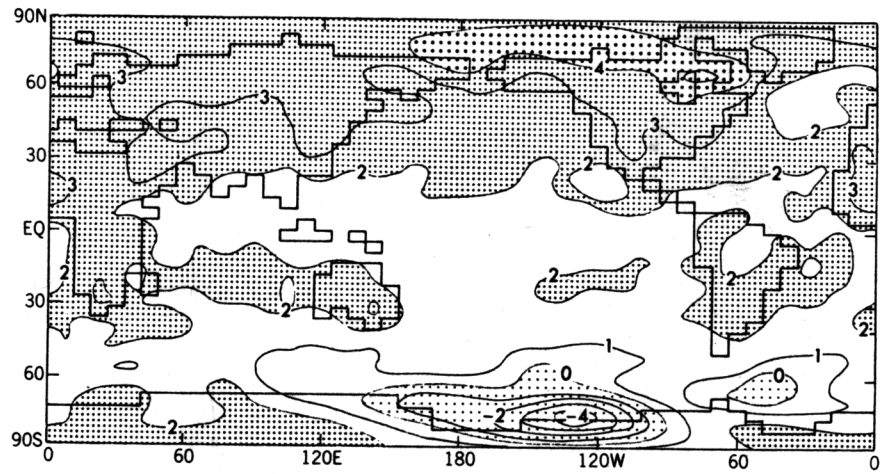

FIG. 3 The geographical distribution of the difference in surface air temperature (°C) between the two integrations averaged over years 61–70.

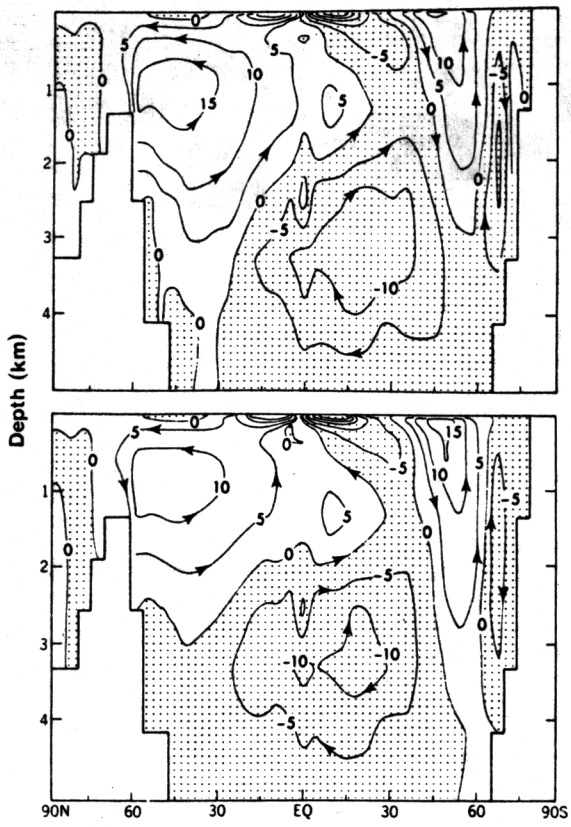

FIG. 4 Streamlines of zonal-mean meridional oceanic circulation (in Sverdrups) averaged over the seventh decade (that is, years 61-70) of the experiment. Top, the control integration with constant CO_2; bottom, the integration in which atmospheric CO_2 concentration is increased with the rate of 1% yr^{-1}.

influence of an abrupt quadrupling of atmospheric CO_2 on the climate of an atmosphere-ocean model with a sector computational domain bounded by the Equator and two meridional boundaries. They found that the thermohaline circulation of the model collapsed completely towards the end of the third decade of the experiment. Washington and Meehl[8] noted that the response of their global model to a linear increase of atmospheric CO_2 was a weakening of the thermohaline circulation in the Atlantic. Manabe and Stouffer[14] found that their global model has two stable equilibria, one with and one without the thermohaline circulation in the Atlantic Ocean. Although we do not observe a complete collapse of the thermohaline circulation here, it is a possibility that deserves[17] further assesment.

In the Southern Hemisphere, the CO_2-induced warming of surface air decreases with increasing latitude in sharp contrast to the situation in the Northern Hemisphere and to the results of equilibrium experiments. The rate of the warming is particularly slow in the Antarctic circumpolar ocean. A similar feature is noted and analysed in studies[6,7] that explored the effect of an abrupt doubling of the atmospheric CO_2 on coupled models with 'sector' and global computational domain, respectively. The latter model is very similar to the present model except that it has annual-mean insolation. The fraction of the area covered by oceans in the Southern Hemisphere is much larger than the corresponding fraction in the Northern Hemisphere. Thus the effective thermal inertia of the Southern Hemisphere tends to be larger than in the Northern Hemisphere[18], accounting for the slower rise of surface air temperature in the former.

Based upon a detailed study of the heat budget[6,7] there is another important mechanism responsible for the interhemispheric difference of effective thermal inertia particularly in high latitudes. From 45°-65° S, the strong surface westerlies induce an Ekman drift current towards the Equator. Because of the absence of a continental barrier in the upper oceanic layer, the zonal pressure gradient is small at the latitudes of the Drake Passage and the southward geostrophic return flow is weak beneath the surface mixed layer. Instead, the surface drift currents are compensated by a deep downwelling north of the Drake Passage gap, southward geostrophic flow at the base of the gap, and deep upwelling south of the circumpolar current, as indicated in Fig. 4. The existence of such an upwelling region is inferred[19,20] from water mass analysis. A deep wind-driven cell is also simulated by eddy-resolving, high-resolution models[21]. In addition to the wind-driven deep cell of meridional circulation described above, we note that (Fig. 4) there is another cell circulating in the reverse direction in the immediate vicinity of Antarctica where deep convective overturning prevails, forming the Antarctic bottom water. These deep cells of meridional circulation together with associated convective overturning and other sub-grid-scale mixing processes enhance the vertical mixing of heat over a thick ocean layer, thereby increasing the effective thermal inertia of the coupled ocean-atmosphere system. This large effective thermal inertia is responsible for the very slow rise of the near-surface temperature in the circumpolar ocean of the model. It is likely that a similar effective vertical mixing is also realized in the actual circumpolar ocean which is characterized by relatively small vertical variations of density and other trace substances such as phosphate and ^{14}C.

The marked interhemispheric asymmetry of our result differs from the study of Schlesinger *et al.*[4] in which an almost symmetric response was obtained. A recent result[8] indicates smaller warming in the Southern than in the Northern Hemisphere. However, the asymmetry is much less pronounced than in the present results. This discrepancy may result from the fact that the wind-driven cell in the circumpolar ocean obtained in the earlier studies is much weaker and shallower than the cell simulated by the present model. Obviously, a careful comparison of results is needed to determine the underlying cause of this discrepancy.

Further evaluation of the mechanisms involved in the effect of ocean circulation on the CO_2-induced climate change is in progress. The general applicability of the present results will be evaluated by conducting further simulations with different rates of CO_2 change and with models of higher computational resolution. □

Received 29 June; accepted 19 October 1989.

1. Bryan, K., Komro, F. G., Manabe, S. & Spelman, M. J. *Science* **215,** 56-58 (1982).
2. Spelman, M. J. & Manabe, S. *J. geophys. Res.* **89,** 571-586 (1984).
3. Bryan, K. & Spelman, M. J. *J. geophys. Res.* **90,** 11679-11688 (1985).
4. Schlesinger, M. E. & Jiang, X. *Climate Dynamics* **3,** 1-17 (1988).
5. Schlesinger, M. E., Gates, W. L. & Han, Y. J. in *Coupled Ocean-Atmosphere Models* (ed. Nihoul, I. C. J.) 447-478 (Elsevier, Amsterdam, 1985).
6. Bryan, K., Manabe, S. & Spelman, M. J. *J. phys. Oceanogr.* **18,** 851-867 (1988).
7. Manabe, S., Bryan, K. & Spelman, M. J. *J. phys. Oceanogr.* (in the press).
8. Washington, W. & Meehl, G. *Clim. Dynamics* **2,** 1-38 (1989).
9. Hansen, J. *et al. J. geophys. Res.* **93,** 9341-9364 (1988).
10. Wetherald, R. T. & Manabe, S. *J. atmos. Sci.* **45,** 1397-1415 (1988).
11. Bryan, K. & Lewis, L. J. *J. geophys. Res.* **84,** 2503-2517 (1979).
12. Ramanathan, V. R., Cicerone, R. J., Singh, H. B. & Kiehl, J. T. *J. geophys. Res.* **90,** 5547-5566 (1985).
13. Bryan, K. *J. phys. Oceanogr.* **14,** 666-673 (1984).
14. Manabe, S. & Stouffer, R. J. *J. Clim.* **1,** 841-866 (1988).
15. Manabe, S. & Stouffer, R. J. *J. geophys. Res.* **85,** 5529-5524 (1980).
16. Manabe, S. & Bryan, K. *J. Geophys. Res.* **90,** 11689-11707 (1985).
17. Broecker, W. S. *Nature* **329,** 123-125 (1987).
18. Thompson, S. L. & Schneider, S. H. *Science* **217,** 1031-1033 (1982).
19. Deacon, G. E. R. *Discovery Rep.* **15,** 125-152 (1937).
20. Sverdrup, H. V., Johnson, M. W. & Fleming, R. H. *The Oceans* (Prentice Hall, Englewood Cliffs, 1942).
21. Semtner, A. J. & Chervin, R. M. *J. geophys. Res.* **93,** 15502-15522 (1988).

ACKNOWLEDGMENTS. We thank I. Held, N.-C Lau, J. D. Mahlman and R. Toggweiler for their comments on the manuscript and J. D. Mahlman for his support.